mAbs

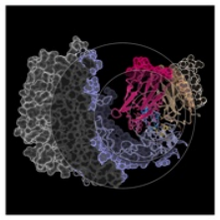

ISSN: 1942-0862 (Print) 1942-0870 (Online) Journal homepage: www.tandfonline.com/journals/kmab20

# A cell line development vector strategy for improved expression of a trispecific T-cell engager in CHO

Rajesh K. Mistry, Chendi Niu, Giulia Lambiase, Daniel Ray, Lewis Kearsey, Noah Hitchcock, Luigi Grassi, Ramy Elgendy, James Fleming, Alexandra C. Broughton, Peng Zhao, Chi-I Chiang, Pooja Shah, Matthew Cyr, Even Walseng, Yariv Mazor, Diane Hatton & Sarah Dunn

**To cite this article:** Rajesh K. Mistry, Chendi Niu, Giulia Lambiase, Daniel Ray, Lewis Kearsey, Noah Hitchcock, Luigi Grassi, Ramy Elgendy, James Fleming, Alexandra C. Broughton, Peng Zhao, Chi-I Chiang, Pooja Shah, Matthew Cyr, Even Walseng, Yariv Mazor, Diane Hatton & Sarah Dunn (2026) A cell line development vector strategy for improved expression of a trispecific T-cell engager in CHO, mAbs, 18:1, 2632994, DOI: 10.1080/19420862.2026.2632994

**To link to this article:** https://doi.org/10.1080/19420862.2026.2632994

MABS
2026, VOL. 18, NO. 1, 2632994
https://doi.org/10.1080/19420862.2026.2632994

Taylor & Francis
Taylor & Francis Group

REPORT

OPEN ACCESS Check for updates

# A cell line development vector strategy for improved expression of a trispecific T-cell engager in CHO

Rajesh K. Mistry[a*], Chendi Niu[b], Giulia Lambiase[c], Daniel Ray[c], Lewis Kearsey[a], Noah Hitchcock[a], Luigi Grassi[a], Ramy Elgendy[d], James Fleming[a], Alexandra C. Broughton[a], Peng Zhao[e], Chi-I Chiang[e], Pooja Shah[e], Matthew Cyr[e], Even Walseng[e], Yariv Mazor[e], Diane Hatton[a], and Sarah Dunn[a**]

[a]Cell Culture and Fermentation Sciences, BioPharmaceutical Development, BioPharmaceuticals R&D, AstraZeneca, Cambridge, UK; [b]Analytical Sciences, BioPharmaceutical Development, BioPharmaceuticals R&D, AstraZeneca, Gaithersburg, USA; [c]Analytical Sciences, BioPharmaceutical Development, BioPharmaceuticals R&D, AstraZeneca, Cambridge, UK; [d]Translational Genomics, Discovery Sciences, BioPharmaceuticals R&D, AstraZeneca, Gothenburg, Sweden; [e]Biologics Engineering, Oncology R&D, AstraZeneca, Gaithersburg, USA

**ABSTRACT**

Recent advances in trispecific antibody (trisAb) engineering offer great therapeutic potential, but achieving high product yield and quality in cell line development remains a challenge due to complex chain pairing requirements in production cell lines. In this study, three distinct expression vector configurations were evaluated for their ability to support robust, high-level expression of a structurally complex, synapse-gated trisAb T-cell engager (TriMab) in stable Chinese hamster ovary cells. Initial configurations using conventional dual heavy chain (HC) and triple light chain (LC) vectors resulted in poor pool performance characterized by delayed transfection recovery and low titers. By contrast, a redesigned strategy that reversed HC gene order and distributed LCs over separate vectors markedly improved transfection recovery along with product titers and reduced the formation of undesired product variants. Clonal cell lines established with this optimized strategy achieved titers exceeding 2 g/L with correct product quality profiles. Gene copy number and mRNA analyses confirmed that chain order and vector design strongly influenced mRNA levels and thus productivity. These results highlight the critical impact of vector configuration on manufacturability of complex TriMabs, providing a practical framework for the rational design of gene vectors to support next-generation trisAb production.

**ARTICLE HISTORY**
Received 27 October 2025
Revised 11 February 2026
Accepted 12 February 2026

**KEYWORDS**
Trispecific antibody; TriMab; T-Cell engager; vector strategy; product quality; Cell line development; Chinese hamster ovary cells

## Introduction

In recent years, novel format multi-specific antibodies that were once considered too challenging to manufacture are beginning to emerge as a leading class of biotherapeutics, with several products approved for marketing.[1–6] These complex modalities differ from conventional monoclonal antibodies (mAbs) in that they can engage several distinct epitopes at once, enabling significantly improved therapeutic potential through expanded functional capabilities.[7,8] Indeed, the enhanced targeting capacity of multi-specific antibodies permits access to unique mechanisms of action such as improved selectivity to double positive cancer cells,[9] half-life extension [10] and targeted T-cell engagement.[11] Despite these advancements, much of this progress in manufacturability has been made in the field of bispecific antibodies with considerable work still to be done on the manufacture of more complex trisAbs.[7]

TrisAbs are structurally diverse with some representing relatively simple, single chain modalities such as the 'beads-on-string' format whereby several single-chain variable fragments are connected via engineered flexible linkers, whereas others represent more complex structures that bear similarity to conventional immunoglobulin G antibodies in that they contain an Fc domain and various antigen-binding fragment (Fab) regions.[6,7] These molecules are often composed of multiple,

**CONTACT** Sarah Dunn sarah.dunn@astrazeneca.com Cell Culture and Fermentation Sciences, BioPharmaceutical Development, BioPharmaceuticals R&D, AstraZeneca, Cambridge Biomedical Campus, 1 Francis Crick Avenue, Cambridge CB2 0AA, UK
*First authorship.
**Senior authorship.

Supplemental data for this article can be accessed online at https://doi.org/10.1080/19420862.2026.2632994.

asymmetric, heterogeneous heavy chains (HCs) and light chains (LCs) that require precise pairing to confer correct functionality. Additional structure-function features can also be engineered into trisAbs to enhance their therapeutic potential; in the context of T-cell engagers, these include synapse AND-gating and cross-arm avidity to enable robust target cell selectivity and reduced off-target effects.[12,13] Whilst these complex structural features are required for functionality and make trisAbs attractive from a therapeutic standpoint, they also pose considerable manufacturability challenges related to stable cell line expression.[14] Indeed, the requirement of the production host cell line to express and subsequently correctly pair a set of disparate antibody chains often leads to aberrant product quality (PQ) and the formation of varied, undesirable mis-paired species.[7,14–16] To facilitate correct chain pairing, antibody engineering strategies can be used, including knobs-into-holes technology (KiH) to enable heterodimeric HC pairing [17] as well as engineered, non-canonical disulfide bonds [18] and electrostatic steering mutations to permit correct LC pairing.[19] It is not uncommon for several of these engineering strategies to be used on a single molecule and, although they confer notable improvements to PQ, they do not completely abrogate the formation of mis-paired species.[19–21] To further complicate protein expression, the presence of mis-paired species within the production cell line can lead to cellular stress responses and poor cell culture performance.[14]

To improve the manufacturability of novel, difficult-to-express (DTE) modalities such as multi-specific antibodies, several cell line development strategies have previously been employed, including the selection of an effective host cell line,[22,23] heterologous expression of chaperone proteins,[24] optimization of culture processes,[25,26] implementation of high throughput screening capabilities,[27] and, importantly, identification of synthetic DNA elements and/or relevant vector configurations.[28,29] The current challenges inherent to the successful manufacture of trisAbs appear to require several molecular and process-based strategies to achieve industrially relevant titers.[26]

Here, we explore the use of varying expression vector configurations for the expression of a complex synapse gated and affinity-tuned TriMab T-cell engager [13] in a stable cell line development workflow. We utilize a combination of stable cell line generation, analytical screening, gene copy number (GCN) and mRNA analysis to identify a vector configuration that can yield clonal cells lines with g/L expression and favorable PQ of this structurally complex TriMab.

## Results

### *TriMab antibody structure*

A schematic of the TriMab T-cell engager used in this investigation is displayed in Figure 1. A detailed description of its structure-function properties is provided by Zhao et al.[13] In brief, the TriMab comprises two asymmetric heavy chains (HC1 hole and HC2 knob) engineered with KiH technology to facilitate correct HC pairing. The hole HC carries an "RF" (H435R/Y436F) mutation that reduces binding of hole–hole dimers to protein A.[30] Correct binding of the three LCs (LC1, LC2 and LC3) to the hole and the knob HCs is facilitated via a combination of electrostatic steering mutations (denoted by -/+ in Figure 1) and site-specific disulfide bonds.

### *Vector approach 1 yields poorly expressing TriMab stable pools*

The TriMab used in this investigation (Figure 1) was predicted to be DTE in stable cell line settings based on data derived from a similar antibody format with heavily engineered structure-function features (data not shown). We therefore aimed to understand how the expression vector configuration can affect TriMab productivity and PQ in stable Chinese hamster ovary (CHO) pools. Initially, we adopted a vector strategy extrapolated from simpler antibody formats: a dual-HC vector (with a glutamine synthase (GS) selection marker) in which the more complex knob HC was positioned upstream of the hole HC, alongside a triple-LC vector (with a puromycin (Puro) selection marker) ordered LC2, LC1, and LC3, as illustrated in Figure 2A. This vector configuration was denoted Vector Approach 1 (VA1). VA1 vectors were stably co-transfected into CHO host cells and recovery monitored over time (Figure 2(B), Supplemental Figure 1(A)).

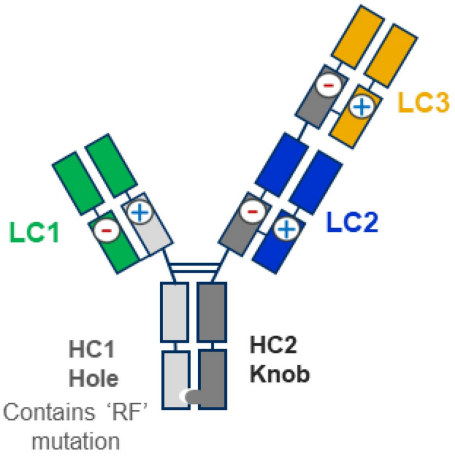


**Figure 1.** Structure of the TriMab antibody used in this Study. A: heavy chain 1 (HC1) is the hole HC (light gray), heavy chain 2 (HC2) is the knob HC (dark gray), knob into hole technology depicted, with 'RF' mutation (reduces binding to protein A) denoted on the hole HC. Light chain 1 (LC1) (green) binds to HC1, light chain 2 (blue) and 3 (yellow) (LC2, LC3) bind to HC2. Charge pairing is illustrated by ± symbols. Disulfide bonds denoted by blue horizontal lines connecting LCs to HCs and HC1 to HC2.

Here, transfection recovery of the TriMab pools was markedly protracted (day 22 recovery) compared to the mAb control vector transfections (day 14 recovery). Interestingly, only VA1 pool 1 and 2 recovered from transfection with VA1 pool 3 displaying viable cell densities (VCDs) equivalent to a $H_2O$ transfected control pool. VA1 pools 1 and 2 were next analyzed for the mRNA expression of all five TriMab chains and corresponding selection markers (Figure 2(C)). Here, both pools display elevated knob HC mRNA compared to hole HC mRNA expression. Additionally, LC1 mRNA was less abundant than LC2 and LC3, which express equivalently within each pool. Notably, pool 1 has higher overall mRNA expression of antibody chains compared to pool 2 despite both pools 1 and 2 having similar mRNA levels of each selection marker.

Pools 1 and 2 were subsequently run in fed-batch and assessed for VCD (Figure 2(D)), viability (Figure 2(E)), lactate (Figure 2(F)) and titer (Figure 2(G)). Here, pool 1 displayed slightly lower growth (pool 1 peak VCD = 13.2x10e6 cells/mL, pool 2 = 18.3x10e6 cells/mL), but higher end-of-run viability compared to pool 2 (pool 1 = 72%, pool 2 = 56%). Lactate levels were comparable between pools and end-of-run (day 11) titer (measured by protein A-mediated detection) was higher for pool 1 compared to pool 2 (pool 1 = 45 mg/L, pool 2 = 23 mg/L, respectively) despite both pools displaying low overall titers compared to a mAb control (average 2047 mg/L) (Supplemental Figure 2). Finally, PQ of purified TriMab (purified by protein A-mediated capture) was assessed using a high throughput screening method for high molecular weight species (HMWS), half knob and knob:knob dimer products (Figure 2(H), Supplemental Figure 3). Here, TriMab produced by pool 1 displayed higher levels of HMWS compared to pool 2 (pool 1 = 8.3%, pool 2 = 4.6%). Of note, half knob (pool 1 = 1.2%, pool 2 = 1%) and knob:knob dimer species (pool 1 = 3.4%, pool 2 = 4.4%) were observed and shown to be comparable between both pools.

### *Vector approach 2: sequential expression of LC and HC vectors yields poorly expressing TriMab stable pools*

Correct folding and processing of antibodies is thought to require excess LC to pair with HC.[31] Given that the TriMab used in this study contains three LC binding domains with additional engineered features to facilitate correct pairing, we hypothesized that the vector transfections for VA1 may lead to a temporal imbalance in LC/HC bioavailability arising from the co-expression of both HC and LC vectors simultaneously. This imbalance may be linked to the poor transfection recovery and subsequent pool performance observed for VA1. To explore this, the triple LC vector was stably transfected into CHO host cells to generate LC-only expressing pools (Supplemental Figure 1(B)) before subsequent transfection with the dual HC vector; this strategy was denoted Vector Approach 2 (VA2) (Figure 3(A)). Here, all three TriMab pools recovered from transfection with an

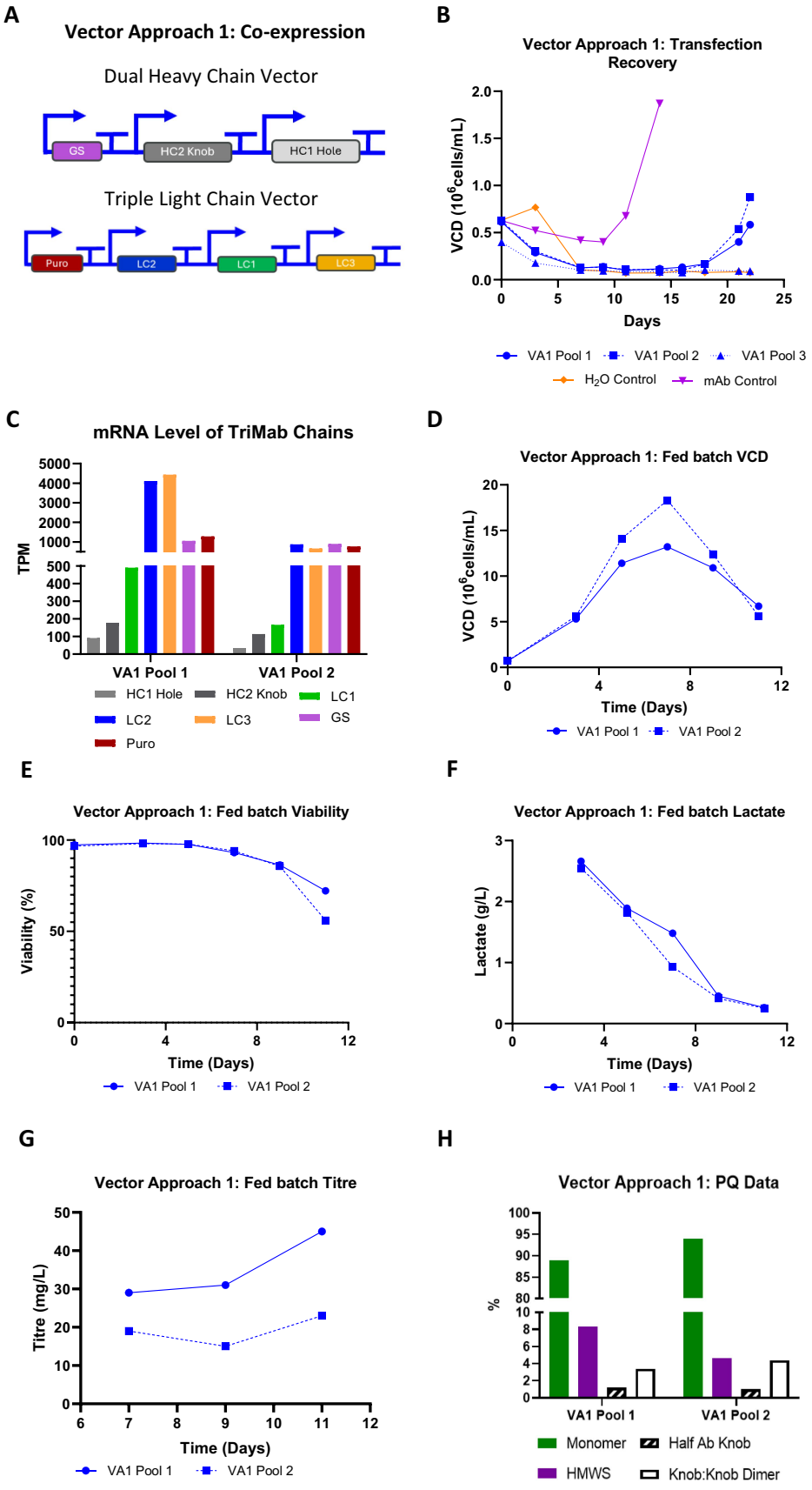


**Figure 2.** Generation and characterisation of stable cell pools expressing a TriMab via vector approach 1 where HC and LC vectors were co-expressed. A: Schematic detailing the vector configuration of antibody chains and selection markers used in vector approach 1 (VA1), glutamine synthase (GS), puromycin (puro), heavy chain (HC), light chain (LC). B: Transfection

extended recovery time (day 19 recovery) compared to mAb control vector transfections (day 14 recovery) (Figure 3B, Supplemental Figure 1(A)).

VA2 pools were next analyzed for the mRNA expression of all five TriMab chains and corresponding selection markers (Figure 3(C)). Here, all three pools display elevated knob HC mRNA compared to hole HC mRNA expression. Additionally, LC1 mRNA was less abundant than LC2 and LC3, which are highly overexpressed in each pool. The puro selection marker displayed increased expression compared to the GS selection marker in pools 1 and 3. VA2 pools were subsequently run in fed-batch and assessed for VCD (Figure 3(D)), viability (Figure 3(E)), lactate (Figure 3(F)) and titer (Figure 3(G)). Here, pool 2 displayed slightly higher growth (pool 2 peak VCD = 9.4x10e6 cells/mL, pool 1 and 3 peak VCD = 7.3x10e6 cells/mL and 7.1x10e6 cells/mL, respectively), but similar end-of-run viability (pool 2 = 37.9%, pool 1 and 3 = 48% and 49%, respectively) and lactate profiles compared to pools 1 and 3. Interestingly, end-of-run titer (day 11) was higher for pools 2 and 3 (pool 2 = 60 mg/L, pool 3 = 56 mg/L) compared to pool 1 (39 mg/L), but all pools displayed low overall titers compared to a mAb control (average 2047 mg/L) (Supplemental Figure S2). Finally, PQ of purified TriMab was assessed using high throughput screening technology for HMWS, half knob and knob:knob dimer products (Figure 3H, Supplemental Figure S3). Here, TriMab produced by pools 1 and 2 displayed higher levels of HMWS (4% and 4.6%, respectively) compared to pool 3 (2.9%). Of note, half knob levels were less abundant in pools 1 and 2 (0.9% and 1.6%, respectively) compared to pool 3 (5.8%) and knob:knob dimer species varied across pools with pool 1 displaying 1.6%, pool 2 displaying the highest level of 4.3% and pool 3 displaying 2.5%.

### *Vector approach 3: reversing the HC order and dividing the LCs across two vectors improves pool performance and product quality*

VA1 and VA2 both utilized the same dual HC vector and triple LC vector from which the hole HC and LC1 displayed decreased mRNA expression compared to other chains (Figures 2C, 3C). Vector approach 3 (VA3) aimed to resolve this by reversing the order of the hole and the knob HCs such that the hole HC was positioned upstream of the knob HC whilst retaining the GS selection marker. In addition, the triple LC vector was divided across two vectors: dual LC vector 1 in which LC3 was now positioned upstream of LC2 whilst retaining the puromycin selection marker and single LC vector 2 in which LC1 was expressed on its own in the absence of a selection marker (Figure 4(A)).

The vectors for VA3 were stably co-transfected into CHO host cells and recovery monitored over time (Figure 4B, Supplemental Figure 1A). Here, all three TriMab pools recovered from transfection with an extended recovery time (day 18 recovery) compared to mAb control vector transfections (day 14 recovery). VA3 pools were next analyzed for the mRNA expression of all five TriMab chains and corresponding selection markers (Figure 4(C)). All three pools displayed elevated expression of hole HC mRNA compared to knob HC mRNA. Additionally, LC1 and LC3 mRNA were more abundantly expressed than LC2 in each pool. The GS selection marker showed lower mRNA expression than the puro marker in pool 1, but equivalent expression in pools 2 and 3.

The VA3 pools were subsequently run in fed-batch and assessed for VCD (Figure 4(D)), viability (Figure 4(E)), lactate (Figure 4(F)) and titer (Figure 4(G)). Pool 1 displayed higher growth (pool 1 peak VCD = 12.8x10e6 cells/mL, pool 2 and pool 3 peak VCD = 8.7x10e6 cells/mL and 7.4x10e6 cells/mL, respectively) and end-of-run viability compared to pools 2 and 3 (pool 1 = 69.2%, pool 2 and 3 = 56.5% and 59.5%, respectively) with all pools showing favorable lactate profiles. Interestingly, end-of-run titer (day 11) was higher for pools 1 and 3 (pool 1 = 187 mg/L, pool3 = 191 mg/L) compared to pool 2 (68 mg/L). Notably, all the VA3 pools displayed higher titers than pools derived from VA1 and VA2, but, despite this

recovery profiles detailing viable cell density (VCD) of pools over time. C: mRNA levels expressed as transcripts per million (TPM) for TriMab chains and selection markers. D: Stable pool VCD over an 11-day fed-batch process. E: Stable pool viability over an 11-day fed-batch process. F: Stable pool lactate over an 11-day fed-batch process. G: Stable pool titer over an 11-day fed-batch process. H: TriMab product quality in protein a purified product showing percentage (%) monomer, high molecular weight species (HWMS), half antibody (ab) knob and knob:knob dimer.

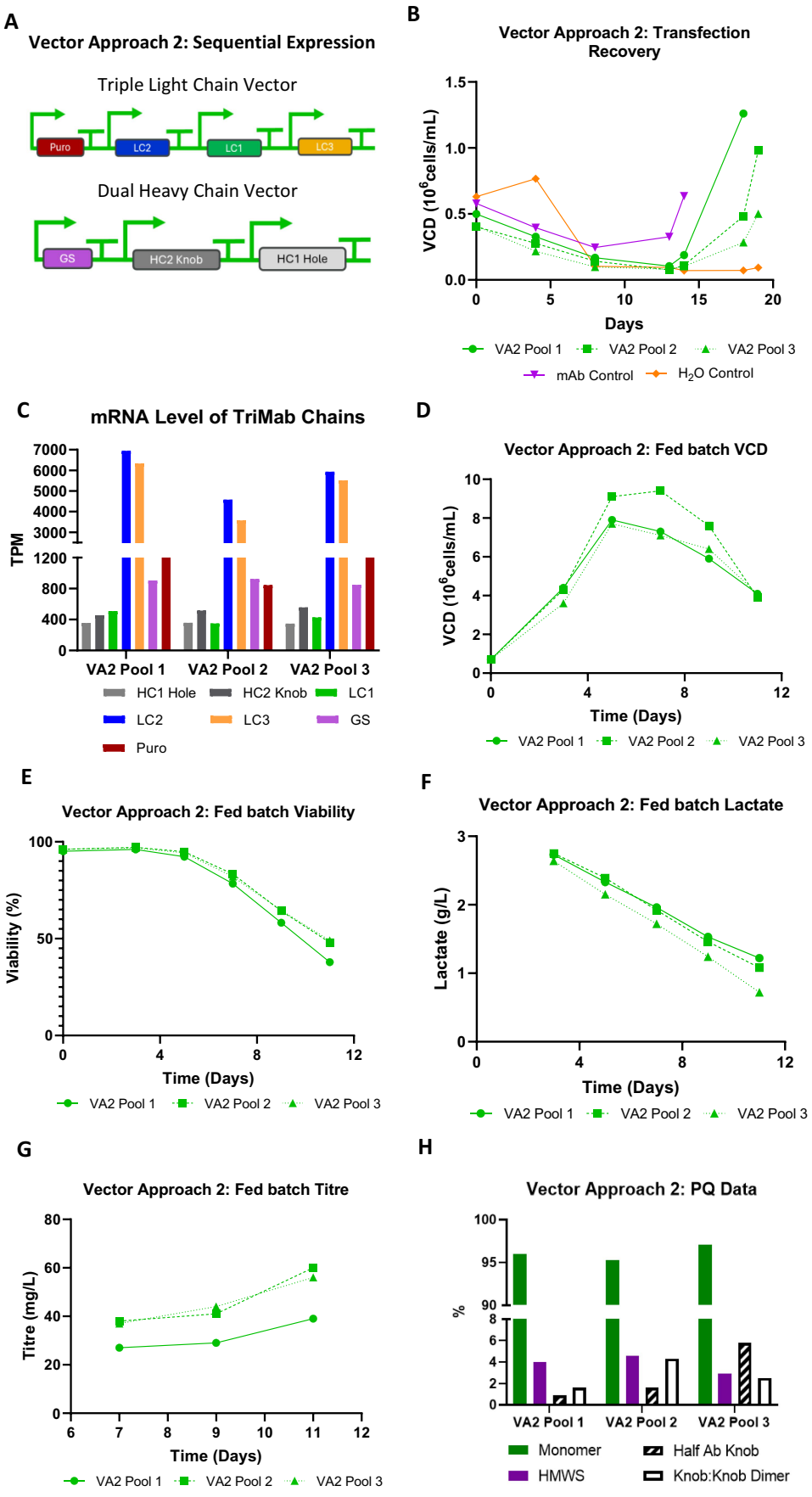


**Figure 3.** Generation and characterisation of stable cell pools expressing a TriMab via vector approach 2 where the LC vector was expressed before the HC Vector. A: Schematic detailing the vector configuration of antibody chains and

overall titer improvement, values were low compared to a mAb control (average 2047 mg/L) (Supplemental Figure 2). Finally, PQ of purified TriMab was assessed using high throughput screening technology for HMWS, half knob and knob:knob dimer products (Figure 4H, Supplemental Figure 3). Here, TriMab produced by pools 1, 2, and 3 displayed HMWS levels of 2.3%, 2.9% and 2.7%, respectively. Strikingly, half knob product was undetected in all 3 pools and knob:knob dimer species were only detected at 0.1% in pool 2, with pools 1 and 3 having an absence of knob:knob dimer.

### *Clonal cell line derivation from vector approaches 1–3 yielded a high proportion of non-TriMab expressing clones*

Clonal cell lines were derived from pools generated using VA1, VA2 and VA3. Of these 117 VA1 clones, 63 VA2 clones and 87 VA3 clones (Supplemental Table 1) were assessed for TriMab production in a high throughput fed-batch screen. Here, average end-of-run VCD for clones derived from each vector approach were comparable (~9x10e6 cells/mL) (Figure 5(A)). However, assessment of end-of-run titer using protein A revealed very few clones expressing detectable levels of the TriMab, 3 ×VA1 clones, 1 ×VA2 clone and 8 ×VA3 clones (Supplemental Table 1). Of these, clones derived from VA1 and VA2 displayed titers below 60 mg/L, by contrast top titer clones derived from VA3 were 1119 mg/L and 804 mg/L (Figure 5(B)). To determine whether the improved titers observed from clones derived from VA3 were due to high clonal cell growth, end-of-run titer data for all clones with detectable titer were plotted against end-of-run VCD (Figure 5(C)), here no correlation was observed between VCD and titer.

Given the high level of clonal cell line attrition, 14 clones were selected, representing all three vector approaches, inclusive of expressing and non-expressing clones, for characterization for mRNA expression (Figure 5(D)) and GCN analysis (Figure 5(E)). Here, analysis of the mRNA expression of all 5 TriMab chains and corresponding selection markers in the 14 clones revealed that all expressing clones (Cl1-10) displayed either knob and hole HC mRNA (VA3 clones 5–10) or only knob HC mRNA (VA1 clones 1–3, VA2 clone 4), compared to non-expressors (Cl11-14), which did not express either knob or hole HC mRNA. Interestingly, all TriMab expressing clones express all 3 LCs along with non-expressing clones 12 and 14, by contrast non-expressing clone 11 shows LC2 and LC3 expression and clone 13 lacks all three LC mRNAs. Both GS and puro selection marker mRNA are expressed in all clones. Analysis of the GCN of all 5 TriMab chains in the 14 clones revealed that all expressing clones (Cl1-10) contain either knob and hole HC gene copies (VA3 clones 5–10) or only knob HC gene copies (VA1 clones 1–3, VA2 clone 4), compared to non-expressors (Cl11-14), which did not contain either knob or hole HC genes. All expressing clones contain all 3 LC genes along with non-expressing clones 12 and 14, by contrast non-expressing clone 11 contains LC2 and LC3 gene copies and clone 13 lacks all TriMab genes.

### *Clonal cell lines derived from vector approach 3 achieved greater than 2 g/L titres in AMBR fed-batch*

Clonal cell lines that were shown to express all five TriMab chains at the mRNA level (VA3 clones 5, 6, 7, 8, 9 and 10) were inoculated into AMBR15 microbioreactors and assessed for VCD (Figure 6(A)), viability (Figure 6(B)), glucose (Figure 6(C)), lactate (Figure 6(D)), titer (Figure 6(E)), and cell specific productivity (qP) (Figure 6F). Here, clone 8 had the highest growth (peak VCD = 24.4x10e6 cells/mL) and clone 10 the lowest growth (peak VCD = 12.3x10e6 cells/mL), with all other clones falling in-between (Figure 6A). All clones displayed an end-of-run viability above 77% apart from clone 10, which fell to 23.8%, clone 8 had the highest end-of-run viability of 91.8% (Figure 6(B)). Clonal cell lines were assessed for metabolism; here glucose consumption was broadly similar across clones (Figure 6(C)) and all clonal lines demonstrated an

selection markers used in vector approach 2 (VA2), glutamine synthase (GS), puromycin (puro), heavy chain (HC), light chain (LC). B: Transfection recovery profiles detailing viable cell density (VCD) of pools over time. C: mRNA levels expressed as transcripts per million (TPM) for TriMab chains and selection markers. D: Stable pool VCD over an 11-day fed-batch process. E: stable pool viability over an 11-day fed-batch process. F: Stable pool lactate over an 11-day fed-batch process. **G**: Stable pool titer over an 11-day fed-batch process. H: TriMab product quality in protein a purified product showing percentage (%) monomer, high molecular weight species (HWMS), half antibody (ab) knob and knob:knob dimer.

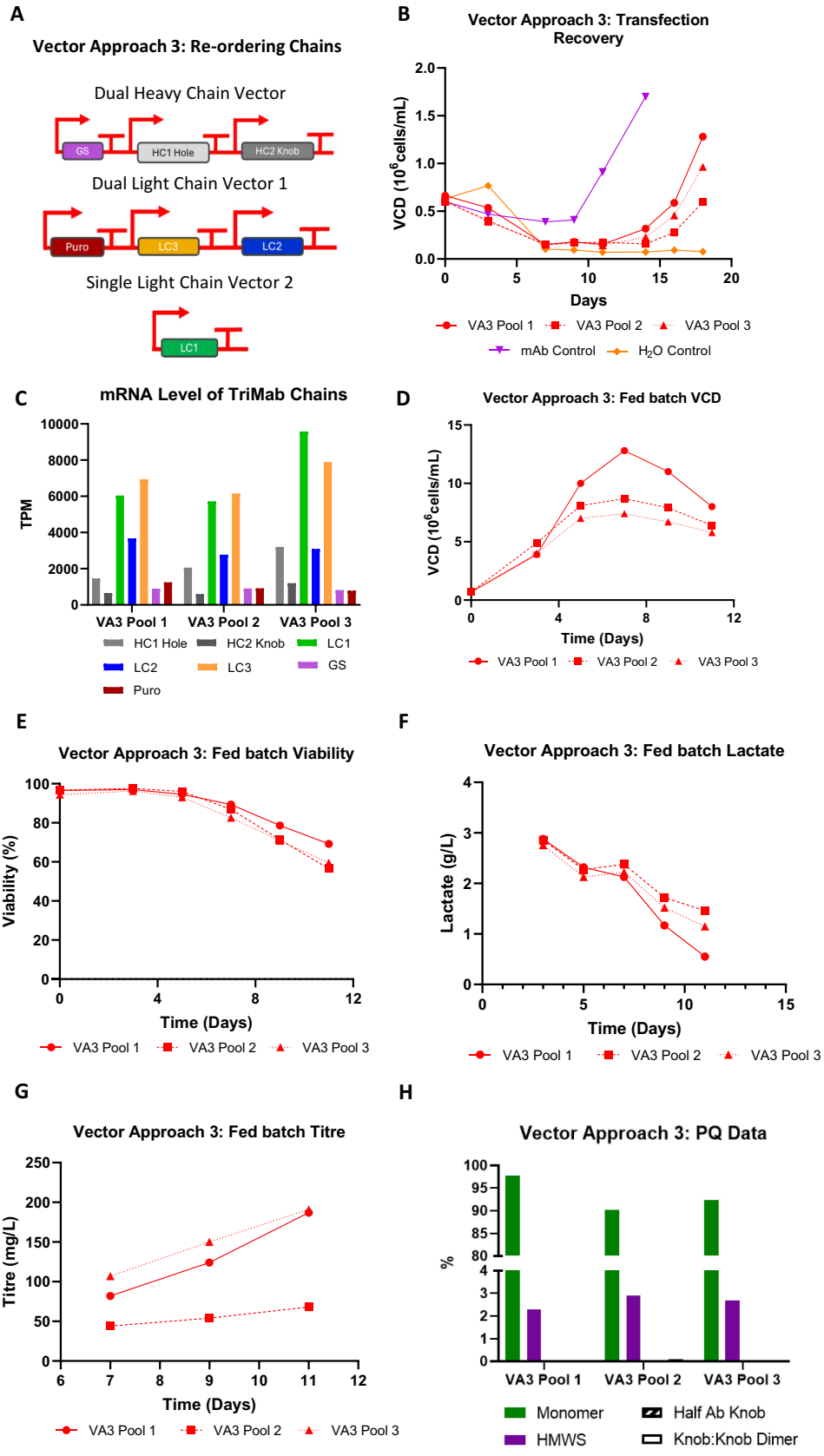


**Figure 4.** Generation and characterisation of stable cell pools expressing a TriMab via vector approach 3 where HC and LC genes were reordered across 3 vectors. A: Schematic detailing the vector configuration of antibody chains and selection markers used in vector approach 3 (VA3), glutamine synthase (GS), puromycin (puro), heavy chain (HC), light chain (LC). B: Transfection recovery profiles detailing viable cell density (VCD) of pools over time. C: mRNA levels expressed as transcripts

ability to back-metabolize lactate. Despite this, clones 8, 9, and 10 had relatively high end-of-run lactate spikes with clone 10 lactate beginning to spike on day 12 (Figure 6(D)). Titer analysis by protein A revealed that clones 7 and 8 had the highest end-of-run titers of 2928 mg/L and 2365 mg/L, respectively. By contrast, clones 5 and 10 had the lowest end-of-run titers of 780 mg/L and 369 mg/L, respectively, whilst clones 6 and 9 achieved end-of-run titers of 1256 mg/L and 1661 mg/L, respectively. Finally, qP was calculated with clone 7 having the highest qP of 23.5 pg/cell/day and clone 5 and 10 having the lowest qP of 5.4 pg/cell/day and 5.3 pg/cell/day, respectively, clones 6, 8 and 9 had qPs of 13.2 pg/cell/day, 13.6 pg/cell/day and 14 pq/cell/day, respectively.

### *TriMab generated by vector approach 3 displays correct product quality*

Finally, PQ, including HMWS, low molecular weight species (LMWS) and chain-mis-paired species were assessed for TriMab purified by protein A-mediated capture from clones 5–9 run in the AMBR15 fed-batch. Here, TriMab produced by clones 6–9 contained lower than 5% HMWS (Figure 7(A)) and lower than 10% LMWS (Figure 7(B)). Intact mass analysis was performed to monitor chain pairing and revealed that clones 6–9 contained above 95% desired chain-pairing species (Figure 7(C)). LC2 and LC3 have only a 25 Da mass difference making it challenging to obtain confident confirmation of correct LC pairing from intact mass analysis. As such, IgdE digested subunit analysis, a method validated to identify 25/26 potential mis-paired species including all LC-duplication variants (e.g., LC1–LC2–LC2), was performed to monitor LC-pairing at the subunit level. This analysis revealed no LC mis-paired species in clones 6–9, implying correct LC pairing. However, in addition to Fc, Fab1 and Fab2 (Supplemental Figure 3), some minor species were also observed in UV profiles (21–22.5 min), which were identified to be either clipped or incompletely digested species, rather than LC mis-paired species (Figure 7(D)). By contrast, clone 5 displayed aberrant PQ with HWMS > 8% (Figure 7(A)) and above 90% LMWS (Figure 7(B)). Intact mass analysis revealed that clone 5 produced ~90% half-knob species and ~10% knob–knob dimers (Figure 7C, Supplemental Figure 3).

## Discussion

Tri-specific antibodies represent an ambitious frontier in the development of protein-based biotherapeutics that have the potential to transform disease outcomes.[6,7] However, the complexity of the structural modifications and features required for molecule functionality presents several critical challenges for manufacturability that arise, in part, due to the necessity for coordinated expression and precise pairing of multiple, non-identical antibody chains within the production host cell line.[15,16] Indeed, gaining fine-tuned control of antibody chain expression through expression vector engineering and optimization has been the focus of much research and has led to improvements in antibody yield and PQ.[28,29,32–36] As such, this study details the systematic evaluation of three distinct vector approaches in stable cell line development to identify a configuration that enables expression of a complex TriMab T-cell engager with industrially relevant, multi-g/L product titers and desirable PQ.

Initial expression efforts, either via co-expression (VA1) or sequential expression (VA2) using a triple LC vector and a dual HC vector, produced stable pools characterized by delayed post-transfection recovery, low productivity, and poor PQ, attributable to the formation of half-knob and knob:knob dimers (see Figures 2B, 2G, 2H, 3B, 3G, 3H). mRNA analysis showed that LC1 was under-expressed relative to LC2 and LC3. This is unlikely to be due to the coding sequence, as the same coding sequence is used in VA3 where LC1 mRNA expression is high. Previous studies have shown that the position of the transgene within the transfected DNA sequence can affect expression levels.[37] It is possible that the position of the LC1 promoter in the vector used in VA1 and VA2, sandwiched between LC2 and LC3 expression cassettes, is limited in its potential to bind transcription factors, resulting in reduced mRNA levels. In VA3 the LC1 promoter is not

per million (TPM) for TriMab chains and selection markers. D: Stable pool VCD over an 11-day fed-batch process. E: stable pool viability over an 11-day fed-batch process. F: Stable pool lactate over an 11-day fed-batch process. G: Stable pool titer over an 11-day fed-batch process. H: TriMab product quality in protein a purified product showing percentage (%) monomer, high molecular weight species (HWMS), half antibody (ab) knob and knob:knob dimer.

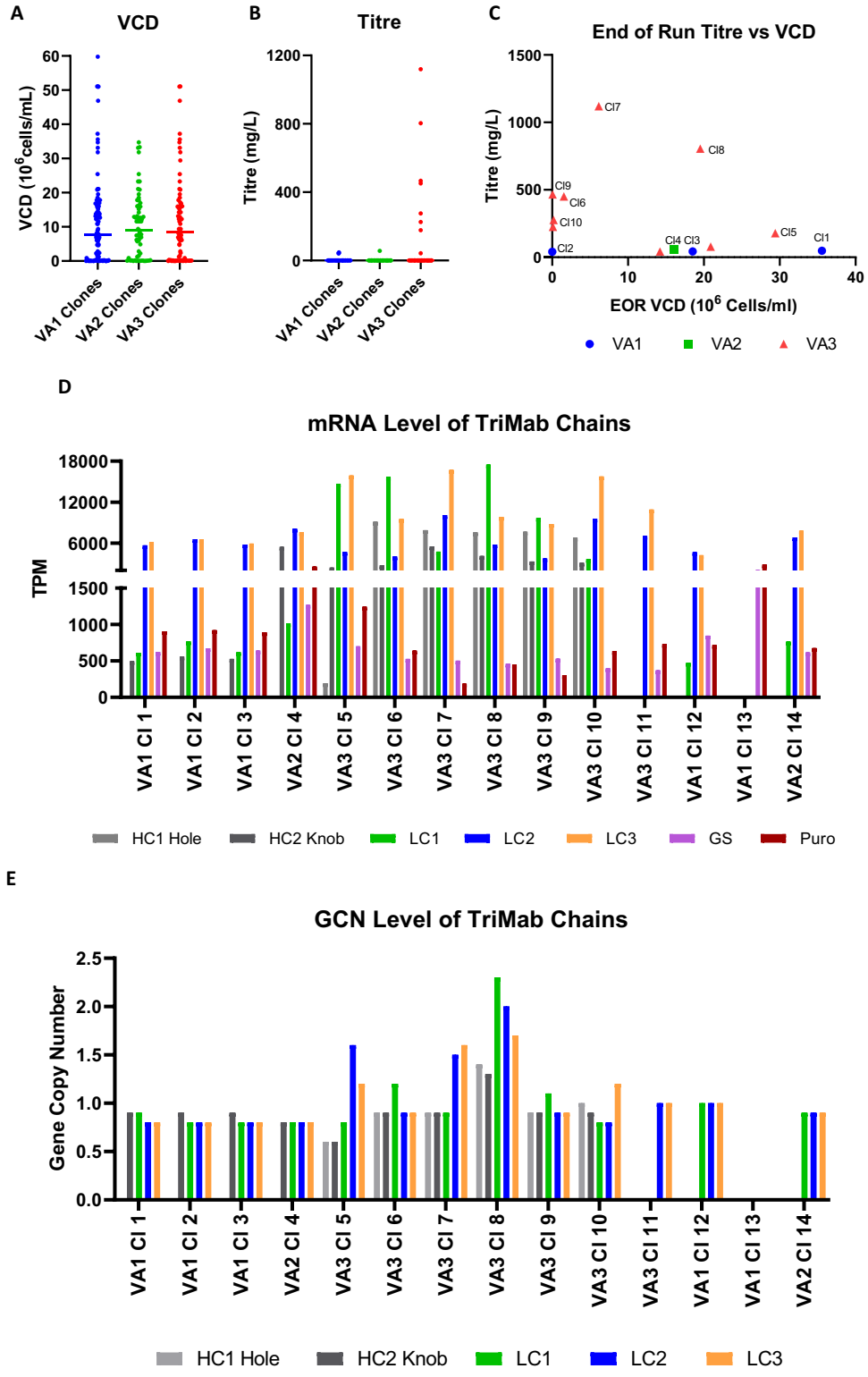


**Figure 5.** Generation and characterisation of clonal cell lines derived from vector approaches 1, 2 and 3. Clonal cell line performance for clones derived from vector approaches 1, 2 and 3. A: End-of -run (EOR) viable cell density (VCD) for clones assessed in shake plate screen. B: EOR titer for clones assessed in shake plate screen. C: Correlation between EOR titer and EOR VCD for expressing clones. D: mRNA levels expressed as transcripts per million (TPM) for TriMab chains and selection markers in expressing and non-expressing clones from each vector approach. E: Gene copy number (GCN) analysis for TriMab chains in expressing and non-expressing clones from each vector approach: glutamine synthase (GS), puromycin (puro), heavy chain (HC), light chain (LC).

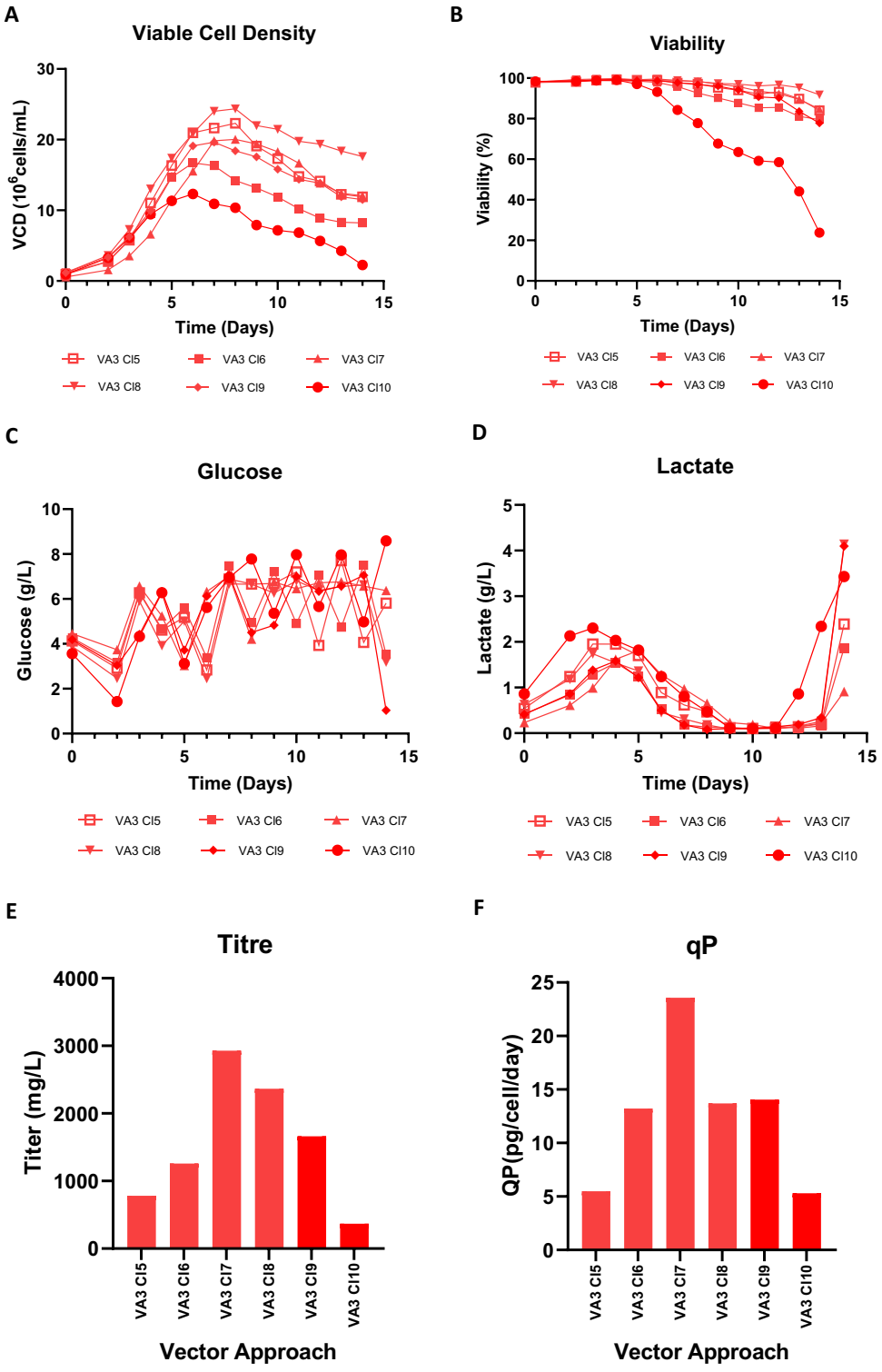


**Figure 6.** Assessment of clonal cell lines derived from vector approach 3 in AMBR15 Bioreactors. Clonal cell line performance for clones 5 -10 from vector approach (VA) 3 over a 14-day AMBR15 fed-batch process. A: Viable cell density (VCD), B: Viability, C: Glucose, D: Lactate, E: Day 14 titer, F: Cell specific productivity (qP).

in close proximity to the promoters of LC2 and LC3 (present on a separate plasmid) and this limitation is alleviated resulting in enhanced LC1 mRNA transcription. Additionally, the knob HC was over-expressed relative to the hole HC (Figures 2C, 3C). Collectively, these data suggest that, despite the use of KiH

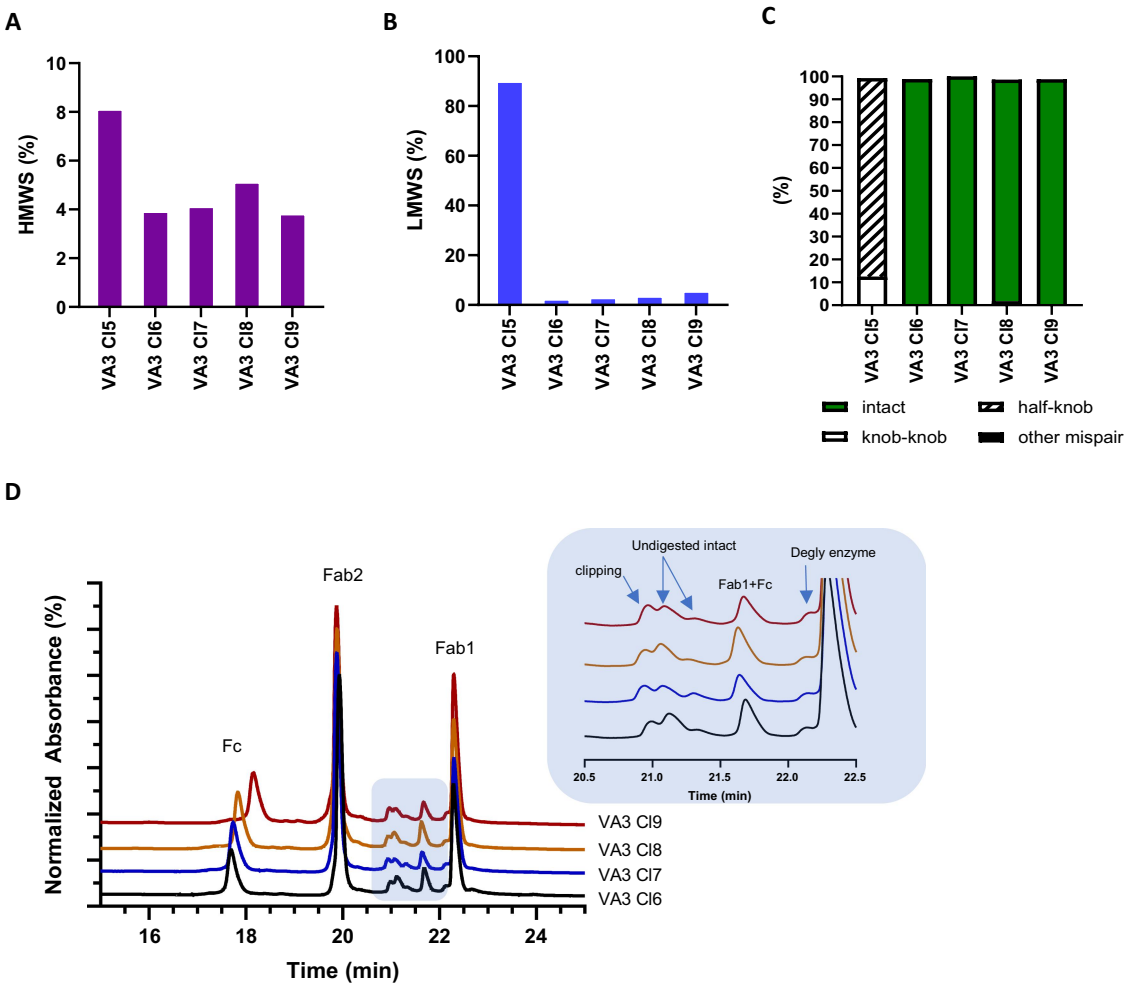


**Figure 7.** Assessment of TriMab product quality for clonal cell lines derived from vector approach 3. Product quality data for TriMab derived from clone 5–9 (Cl5-9) produced from vector approach (VA) 3. A: High molecular weight species levels (% HMWS) by SEC, B: Low molecular weight species levels (%LMWS) by GXII-CE-SDS, C: Chain-pairing analysis by intact LC-MS analysis, D: Light chain (LC) pairing confirmation by subunit LC-MS analysis for clones 6–9. Fab1 = hole fd + LC1; Fab2 = knob fd + LC2 + LC3; Fab1 + Fc = incomplete digested species with only Fab2 removed; degly enzyme = PNGase F.

mutations to drive correct HC pairing, imbalanced HC and LC gene expression can also influence overall PQ.

By contrast, VA3, which reordered genes such that the hole HC (HC1) was upstream of the knob HC (HC2) and the LC cassette was split between a dual LC vector (LC3, LC2) and a single LC vector (LC1), substantially improved pool performance, including transfection recovery, titer, and PQ. mRNA profiling revealed increased hole HC (HC1) expression relative to knob HC (HC2), while placing LC1 on a separate vector dramatically boosted LC1 mRNA levels. This configuration not only improved titer, but also resulted in near-complete elimination of half knob and knob:knob dimer species (Figure 4(H)). These findings align with prior reports that antibody chain gene order and transcriptional output affect productivity and PQ for mAb and bispecific formats.[34,37] In VA1 and VA2, HC1 and LC1, comprising half of the TriMab (Figure 1), showed low mRNA transcript levels, yielding an overabundance of unpaired knob HC and poor PQ (Figures 2H, 3H). Mis-paired species are known to elicit cellular stress responses.[14] We propose that HC gene order drives protein folding burden during post-transfection recovery: in VA1/VA2, elevated knob HC transcript correlates with unpaired knob HC protein, which likely increases stress and selection stringency, enriching for low/non-producers and capping HC transcript levels, whereas in VA3, placing the hole HC first may facilitate folding/assembly, reduce stress, and permit higher HC transcription (consistent with elevated HC1 hole mRNA). As such, to enhance pool robustness, an inducible system that suppresses DTE chain expression during transfection recovery may be beneficial, as shown by Maltais et al. [35]

To assess clonal cell performance, clones were derived across all three vector approaches and screened for TriMab production. Here, a strikingly low proportion of clones showed expression of the TriMab (Supplemental Table 1). Consistent with stable pool data, only clones derived from the VA3 pools displayed volumetric titers above 100 mg/L with the top clones achieving 1119 mg/L and 804 mg/L. These data are in line with findings by Peltret *et al.* who observed high levels of low producer DTE trisAb clones in a non-optimized process.[26] It is noteworthy that the TriMab used in this study contains an 'RF' mutation in the hole HC, which reduces binding of hole-hole dimer species to protein A [38] (Supplemental Figure 3). Since protein A was used for titer analysis as well as for TriMab purification prior to PQ assessment, hole-hole dimers were potentially lost during protein A capture and therefore not detected in the subsequent titer or intact mass analysis. As such, non-expressors may in fact be expressing hole-hole dimers although this does not appear to be the case for non-expressing clones assessed for GCN and mRNA levels.

To explore the potential mechanism underpinning expressing vs non-expressing clones, GCN and mRNA expression profiles were evaluated for 14 representative clones. Analysis of mRNA expression showed that all clones with detectable titer levels (Cl1–10) displayed either both knob and hole HC mRNA (VA3 clones 5–10) or only knob HC mRNA (VA1 clones 1–3; VA2 clone 4), whereas non-expressors failed to express both knob or hole HC mRNA (Figure 5(D)). Moreover, mRNA data was corroborated by GCN findings, which revealed that the differences in TriMab chain expression between clones occurred because of either preferential outgrowth of clones that lacked hole expression, or the loss of the stably integrated antibody chain genes as opposed to other mechanisms such as gene silencing (Figure 5(E)). Interestingly, VA3, which involved the use of LC1 on a vector with no selection marker, appears to integrate in a phenotypically stable manner, as all clones derived from VA3 apart from clone 11 have detectable gene copies and expression of LC1. Despite this, future work exploring expression stability of all antibody chains in aged cell banks will help confirm phenotypic stability.

Finally, an assessment of top clones in AMBR fed-batch revealed expression titers exceeding 2 g/L for clones 7 and 8 (Figure 6(E)) along with desirable cell culture parameters including end-of-run VCD; these data suggest that the low end-of-run VCDs observed for VA3-derived clones at the clone screening stage (Figure 5C) likely reflects the impact of the scale-down screening model rather than intrinsic growth limitations, as these were not observed in the AMBR fed-batch. Assessment of PQ using intact mass and IgdE subunit analysis demonstrated that, post-purification, clones generated intact and correctly paired TriMab product with minimal HMWS and LMWS (Figure 7A-D, Supplemental Figure 4A-E). However, to definitively confirm correct chain pairing non-reduced peptide mapping would need to be implemented in future studies. These data demonstrate that VA3 not only yields industrially relevant titers, but can deliver correct PQ for this complex TriMab modality.

Collectively, these data emphasize the strong influence that vector configuration has on TriMab expression and the critical need to identify vector configurations that enable balanced and robust expression of all antibody chains. Moreover, extensive clone screening and rigorous PQ evaluation remain integral to the successful establishment of a stable manufacturing cell line for TriMabs. Based on the study presented here, we recommend VA3 as the starting vector configuration for the expression of TriMabs, which can be iterated into new configurations for parallel screening and further optimization according to the needs of the TriMab being expressed. Future studies may also benefit from integrating additional approaches such as promoter tuning,[28] translational regulation,[39] site-specific integration [40] or transposon technology,[41] optimized host cell lines,[22,23] and improved bioprocess parameters and production conditions to further improve TriMab productivity and homogeneity as illustrated by Peltret *et al.* [26] Overall, our stepwise vector engineering strategy enabled the establishment of stable CHO cell lines capable of producing a structurally complex, synapse-gated and affinity-tuned TriMab with industrially relevant titers and correct PQ. This study establishes a framework for the rational design of gene expression vectors for complex trisAbs and contributes toward ongoing efforts in the industrialization of these next-generation biotherapeutics.

## Materials and methods

### Methods

#### Cell lines and culture conditions

AstraZeneca proprietary CHO host cells, a suspension-adapted CHO-K1 derivative, were maintained in CD CHO medium (Life Technologies) supplemented with 6 mM L-glutamine (Life technologies) and sub-cultured every 3 - 4 days at a seeding density of 0.2 - 0.3 × 10e6 cells/mL. Stably transfected CHO cell pools and clones were routinely maintained in AstraZeneca proprietary chemically-defined (CD) medium. Routine culture for all cell lines was performed at 36.5°C in vented, non-baffled Erlenmeyer flasks (Corning, Amsterdam, The Netherlands), in 6% $CO_2$ maintained at 140 rpm. Cells were sub-cultured every 3 - 4 days at a seeding density of 0.3 - 0.4 × 10e6 cells/mL. Viable cell density (VCD) and cell viability were assessed using a Vi-Cell XR automated cell counter and viability analyzer (Beckman Coulter, High Wycombe, UK).

#### Vector construction

Expression plasmids encoding the TriMab and a control monoclonal antibody (mAb control) were constructed using restriction enzyme digestion and ligation methods. The control mAb vector comprised a single expression plasmid containing a HC and a LC sequence and a GS selection marker. For the TriMab molecule, each chain was expressed as a single transcriptional unit, flanked by a promoter, 5' untranslated region and poly-adenylation sequence. Puromycin resistance (Puro) and GS genes were encoded into vectors as selectable markers. Several iterations of the TriMab vector were constructed and are detailed in Figure 2A and 4A. In each iteration tested, the order of the gene sequences was changed, not the nucleotide sequence or surrounding promoter, 5' untranslated region or poly-adenylation sequence. The TriMab structure is shown in Figure 1. Heterodimerisation of the two distinct HCs is achieved by KiH mutations in the constant heavy chain 3 domains.[42] HC1 contains the "hole" mutations (T366S, L368A, and Y407V), heterodimer disulfide (Y349C) mutation and RF mutations (H435R/Y436F). HC2 contains the "knob" mutation (T366W) and a heterodimer disulfide mutation (S354C). Cognate HC and LC pairing is achieved via an engineered interchain disulfide bond in one of the constant heavy 1 (CH1)-constant light chain (CL) domains combined with electrostatic steering mutations at the interface of both CH1-CL domains.[19,38] The Fab region formed from HC1 (hole) and LC1 (kappa) carries a wild-type interchain disulfide bond and electrostatic steering mutations (S183K in CH1 and V133E in kappa LC) to promote correct LC-HC pairing. The Fab region formed from HC2 (knob) and LC2 (lambda) possesses an engineered interchain disulfide bond (F126C, C220V in CH1 and S122C, C212V in lambda LC) and electrostatic steering mutations (A141D in CH1 and T117R in lambda LC) at the CH1-CL interface. The Fab region formed from HC2 (knob) and LC3 (kappa) features an engineered interchain disulfide bond (F126C, C220V in CH1 and S121C, C214V in kappa LC3) and electrostatic steering mutations (S183E in CH1 and V133K in kappa LC) at the CH1-CL interface.

#### Stable pool generation

Stable transfectant pools expressing each vector combination (detailed In Figures 2A, 3 A and 4A) were generated using the Amaxa™ Nucleofector™ system (Lonza, Basel, Switzerland) with the Cell Line Nucleofector® Kit V (Lonza) as per manufacturer's instructions. The transfected cells were selected in medium containing methionine sulfoximine (MSX) and/or puromycin (depending on the selection marker of the transfected vector(s)). Cell viability and VCD were monitored on a Vi-Cell XR automated cell counter (Beckman Coulter, High Wycombe, UK) until cells recovered, successful recovery was achieved when cells reached a VCD of ≥0.5 × 10^6 cells/mL post transfection.

#### Clonal cell line generation

Prior to single-cell cloning, 384-well plates (Corning) were filled with proprietary medium supplemented with MSX using a Multidrop Combi reagent dispenser (ThermoFisher Scientific). For single-cell cloning, each CHO pool to be cloned was sorted by depositing single cells into individual wells of pre-filled 384-well plates using the f.sight single-cell printer (Cytena, Germany). All plates were then

incubated at 36.5°C in a humidified incubator with 6% $CO_2$ for 11 - 14 days before cell confluence was measured on a Cellavista imager (Synentec GmbH; data not shown). Clones were expanded into flat bottom 96-well plates (Corning) and then into 96 deep well (96DW) 2 mL Masterblock plates (Greiner Bio-one) using a Hamilton-Star liquid handler (Hamilton, Reno, NV, USA). Selected clones were scaled up from 96DW plates into 24 square well, V-bottom 10 mL/well polypropylene plates (Porvair Sciences) and then into Erlenmeyer flasks (Corning).

### Fed-batch culture

Antibody production was evaluated by fed-batch culture either in an AMBR15 system (Sartorius, UK), 250 mL Erlenmeyer flasks or 96DW plates.[43] The production cultures grew at 36.5°C for 14 days for AMBR15 fed-batch, 11 days for flask-based fed-batch or 10 days for 96DW plate fed-batch. The flasks and 96DW cultures were maintained in a humidified 6% $CO_2$ atmosphere at a shaker speed of 140 rpm for flasks and 350 rpm for 96DW plates. Cell density and viability were monitored during cultivation in flasks, but not for the 96DW cultures, where an end-of-run, day 10 cell count was performed. For flasks, culture medium was supplemented with bolus additions of a proprietary nutrient feed over the course of the fed-batch process with lactate and glucose monitored using a YSI (2900D, YSI Inc). For 96DW plates, culture medium was supplemented with bolus additions of a proprietary nutrient feed and glucose over the course of the fed-batch process. For the AMBR15 fed-batch system, settings of 35.5°C, 900 to 1500 rpm, 50% dissolved oxygen and pH 7.0 ± 0.1 were monitored and regulated. In addition, fresh cell samples were collected every day from the AMBR15 bioreactors for offline measurement of pH, gases ($pCO_2$ and $pO_2$), lactate and glucose levels, VCD, and cell viability using a BioProfile FLEX2 (Nova Biomedical, MA). Proprietary feed was added periodically to the production cultures. Antibody titers in the culture supernatant were determined using Protein A (PA) biosensors in an Octet QK384 (Pall ForteBio, Fremont, CA) for 96DW and by PA HPLC (Agilent Technologies, CA) for AMBR15 and flask cultures. Cell-specific productivity (qP) was calculated as follows: qP = Th/CCTf (where Th is the harvest titer and CCTf is calculated cumulative cell time on the last day of the culture). CCTi = ((di – di-1) X (VCNi + VCNi-1)/2) + CCTi-1 (where d is the day of the culture, VCN is the viable cell count and i is the day of VCN sampling during the culture).

### High throughput purification

Purification was performed using PhyTip 200 µL columns containing 20 µL of ProPlus (MabSelect SuRe™) affinity resin (Biotage) operated on a Tecan Freedom EVO® 200 robotic liquid handling platform with Freedom EVOware®, Version 2.7 (TECAN Group Ltd.). Gibco™ 1x Dulbecco's phosphate-buffered saline (DPBS; Thermo Fisher Scientific) was used for column equilibration and 25 mM sodium acetate, 120 mM sodium chloride buffer pH 5.5 for wash steps. Samples were eluted using 100 mM glycine buffer pH 2.7 and neutralized by the addition of 1 M Tris pH 7.5. Product purification from cultures of the top clones was performed using IMCS MabSelect Sure ProA tips on a Hamilton Star liquid handling robot. 50 mM Tris buffer (pH 7.4) was used for resin equilibration and 1x PBS buffer was used for washing. Samples were eluted using Thermo IgG elution buffer and neutralized with 1 M Tris pH 8.0. Presence of the RF mutation in HC1 is anticipated to ablate binding of half-hole or hole-hole dimer mis-paired species to protein A.

### Intact and subunit mass analysis

Samples were deglycosylated by PNGaseF (Promega) before intact mass analysis. Samples were subjected to overnight FabAlactica (IgdE, Genovis) digestion before subunit mass analysis. Deglycosylated or IgdE digested protein samples were injected into a BioResolve™ mAb Polyphenyl reversed phase column (450Å, 2.7 µm, Waters) on a UPLC (Waters), before being introduced to a Q-Exactive HFX mass spectrometer (Thermo). Mobile phases A and B were 0.1% trifluoroacetic acid in water and in acetonitrile, respectively. Mass spectra were collected at a mass-to-charge ratio range of 800–4500. Mass deconvolution was performed using Byos (Protein Metrics Inc.).

### Size exclusion chromatography

Size exclusion chromatography (SEC) was performed to analyze HMWS. Purified protein samples were injected into a Protein BEH SEC column (200 Å, 4.6 mm ×150 mm, Waters). Proteins were eluted isocratically by using sodium phosphate buffer at 0.5 mL/min flow rate on an Agilent 1260 HPLC system. Any peaks eluting before the major product peak were integrated as HMWS.

### RNA sample preparation and transcriptomic sequencing

Samples for transcriptomic analysis were collected during routine culture of both pooled and clonal cell lines. Aliquots containing $10 \times 10^6$ cells were harvested by centrifugation at 130 *g* for 5 minutes. The supernatant was discarded, and the resulting pellet was resuspended in 200 µL RNAlater® (Sigma-Aldrich) and stored at – 80°C. Following removal of RNAlater, pellets were treated with a lysis buffer containing Proteinase K from an RNAdvance Tissue kit (Beckman Coulter). Samples were vortexed and incubated at 37°C for 25 minutes. RNA extraction was carried out on a Biomek i7 Hybrid robotic workstation (Beckman Coulter) according to the manufacturer's protocol. mRNA enrichment and sequencing library preparation were performed using a KAPA mRNA HyperPrep Kit (Roche) on a Tecan Fluent® liquid handler, following the manufacturer's instructions. Library quality and integrity were assessed with an SS NGS fragment kit (1–6000 bp; Agilent) on a fragment analyzer. Sequencing was conducted on an Illumina NextSeq 2000 platform using paired-end 2 × 110 bp reads and a 200-cycle P3 Reagent Kit (Illumina).

### RNA-seq data analysis

For cell pool and clone RNA-seq processing, Fastp,[44] version 0.23.4, with parameters "–compression 9 –detect_adapter_for_pe – qualified_quality_phred 15 –unqualified_percent_limit 10 –average_qual 20 –length_required 30," was used to trim PCR and sequencing adapters and filter low quality read pairs. Trimmed and qc-filtered reads were then used with Salmon,[45] version 1.10.0, with the selective alignment strategy [46] and the parameters "–libType A – mimicStrictBT2," to quantify the expression of transcripts, annotated in Ensembl, version 93,[47] with the addition of the extra transgenes. The Bioconductor package txtimport [48] was used to summarize transcript expression into gene expression.[49–53]

### Gene copy number analysis

Genomic DNA was extracted from clonal cell lines using a PureLink™ Genomic DNA kit (Invitrogen) according to the manufacturer's protocol. GCN analysis was carried out on Not1-digested genomic DNA from each sample using a TaqMan Assay System with probes designed against antibody encoding DNA sequences (Supplemental Table 2) (Thermo Fisher Scientific) and a Q×100 Droplet Digital PCR System, along with QuantaSoft software (BioRad). Manufacturer's instructions were followed throughout.

## Abbreviations

| | |
|---|---|
| Ab | antibody |
| AMBR | automated microbioreactor |
| bp | base pair |
| CCT | cumulative cell time |
| CD | chemically defined |
| CE-SDS | capillary electrophoresis–sodium dodecyl sulfate |
| CH1 | constant heavy chain 1 |
| CHO | Chinese hamster ovary |
| CL | constant light chain |
| CLD | cell line development |
| DNA | deoxyribonucleic acid |
| DPBS | Dulbecco's phosphate-buffered saline |
| DTE | difficult to express |
| EOR | end of run |
| Fab | fragment antigen-binding |
| Fc | fragment crystallizable – antibody constant region |
| Fd | heavy-chain fragment of Fab |
| GCN | gene copy number |

| | |
|---|---|
| GS | glutamine synthetase |
| HC | heavy chain |
| HFX | high-field Orbitrap mass spectrometer |
| HMWS | high molecular weight species |
| HPLC | high-performance liquid chromatography |
| IgdE | immunoglobulin-degrading enzyme |
| IMCS | Integrated Micro-Chromatography Systems |
| KiH | knobs-into-holes |
| LC | light chain |
| LC-MS | liquid chromatography–mass spectrometry |
| LMWS | low molecular weight species |
| mAb | monoclonal antibody |
| mRNA | messenger ribonucleic acid |
| MSX | methionine sulfoximine |
| NGS | next-generation sequencing |
| PA or ProA | Protein A |
| PBS | phosphate-buffered saline |
| PCR | polymerase chain reaction |
| pCO2 | partial pressure of CO2 – process parameter |
| pH | hydrogen ion concentration measure – process parameter |
| PNGase F | peptide-N-glycosidase F – deglycosylation enzyme |
| pO2 | partial pressure of O2 – process parameter |
| PQ | product quality |
| Puro | puromycin |
| qP | cell-specific productivity |
| SEC | size-exclusion chromatography |
| TPM | transcripts per million |
| TriMab | trispecific antibody T-cell engager |
| TrisAb | trispecific antibody |
| UPLC | ultra-performance liquid chromatography |
| UV | ultraviolet |
| VA | vector approach |
| VCD | viable cell density |
| VCN | viable cell number |

## Acknowledgments

The authors thank Fabio Zurlo and the Bioprocess Analytics team for HPLC and Octet titer analysis, Brendan Grimes and Ivy Kabundi for antibody purification, Lisa Ding for plasmid construction and the Cell Line Development team at AstraZeneca for their support and valuable discussion.

## Author contribution statement

R.K.M. and S.D. conceived the project, conceptualized and designed the experiments. R.K.M. performed cell line generation and characterization experiments. L.K. designed and generated expression vectors. J.F. and N.H. designed and performed GCN analysis. G.L., D.R., and C.N. performed product quality analysis. R.E. performed RNA extraction and library preparation. L.G. performed transcriptomics and bioinformatics analysis. A.C.B. generated preliminary scoping data. R.K.M. and S.D. wrote and reviewed the manuscript. P.Z., C.C., P.S., M.C., E.W., and Y.M. designed the molecule and provided scientific and strategic input. D.H. reviewed the manuscript. OpenAI GPT-5 was used for structuring the text under the supervision of the R.K.M.

## Disclosure statement

The authors declare the following financial interests/personal relationships which may be considered as potential competing interests: This work was supported by Biopharmaceutical Development, AstraZeneca. Authors R.K.M., C. N., D.R., L.G., R.E., J.F., P.Z., C.C., P.S., M.C., E.W., D.H., and S.D. are employees of AstraZeneca and have stock and/or stock interests or options in AstraZeneca. L.K., A.B., G.L., and Y.Z. were employed by AstraZeneca at the time the work was completed.

## Funding

Funding was provided by AstraZeneca.

## ORCID

Rajesh K. Mistry http://orcid.org/0000-0002-9992-8735

## Data and materials availability

All data are available in the main text or the supplementary materials.

## References

1. Cho BC, Simi A, Sabari J, Vijayaraghavan S, Moores S, Spira A. Amivantamab, an epidermal growth factor receptor (EGFR) and mesenchymal-epithelial transition factor (MET) bispecific antibody, designed to enable multiple mechanisms of action and broad clinical applications. Clin Lung Cancer. 2023;24(2):89–97. doi: 10.1016/j.cllc.2022.11.004.
2. Goebeler ME, Bargou R. Blinatumomab: a CD19/CD3 bispecific T cell engager (BiTE) with unique anti-tumor efficacy. Leuk Lymphoma. 2016;57(5):1021–1032. doi: 10.3109/10428194.2016.1161185.
3. Jen EY, Xu Q, Schetter A, Przepiorka D, Shen YL, Roscoe D, Sridhara R, Deisseroth A, Philip R, Farrell AT, et al. Fda approval: Blinatumomab for patients with B-cell precursor acute lymphoblastic leukemia in morphologic remission with minimal residual disease. Clin Cancer Res. 2019;25(2):473–477. doi: 10.1158/1078-0432.CCR-18-2337.
4. Knight T, Callaghan MU. The role of emicizumab, a bispecific factor IXa- and factor X-directed antibody, for the prevention of bleeding episodes in patients with hemophilia A. Ther Adv Hematol. 2018;9(10):319–334. doi: 10.1177/2040620718799997.
5. Sahni J, Patel SS, Dugel PU, Khanani AM, Jhaveri CD, Wykoff CC, Hershberger VS, Pauly-Evers M, Sadikhov S, Szczesny P, et al. Simultaneous inhibition of angiopoietin-2 and vascular endothelial growth factor-A with faricimab in diabetic macular edema: boulevard phase 2 randomized trial. Ophthalmology. 2019;126(8):1155–1170. doi: 10.1016/j.ophtha.2019.03.023.
6. Tapia-Galisteo A, Compte M, Álvarez-Vallina L, Sanz L. When three is not a crowd: trispecific antibodies for enhanced cancer immunotherapy. Theranostics. 2023;13(3):1028–1041. doi: 10.7150/thno.81494.
7. Keri D, Walker M, Singh I, Nishikawa K, Garces F. Next generation of multispecific antibody engineering. Antibody Ther. 2023;7(1):37–52. doi: 10.1093/abt/tbad027.
8. Brinkmann U, Kontermann RE. The making of multispecific immunoglobulins – a clinical perspective. MAbs. 2026;18(1):2613548. doi: 10.1080/19420862.2026.2613548.
9. Mazor Y, Sachsenmeier KF, Yang C, Hansen A, Filderman J, Mulgrew K, Wu H, Dall'acqua WF. Enhanced tumor-targeting selectivity by modulating bispecific antibody binding affinity and format valence. Sci Rep. 2017;7(1):40098. doi: 10.1038/srep40098.
10. Pilati D, Howard KA. Albumin-based drug designs for pharmacokinetic modulation. Expert Opin Drug Metab Toxicol. Expert Opin Drug Metab Toxicol. 2020;16(9):783–795. doi: 10.1080/17425255.2020.1801633.
11. Zhou S, Liu M, Ren F, Meng X, Yu J. The landscape of bispecific T cell engager in cancer treatment. Biomark Res. 2021;9(1):38. doi: 10.1186/s40364-021-00294-9.
12. Seung E, Xing Z, Wu L, Rao E, Cortez-Retamozo V, Ospina B, Chen L, Beil C, Song Z, Zhang B, et al. A trispecific antibody targeting HER2 and T cells inhibits breast cancer growth via CD4 cells. Nature. 2022;603(7900):328–334. doi: 10.1038/s41586-022-04439-0.
13. Zhao P, Schardt J, Chiang C-I, Shah P, Eun GS, Martinek J, Cyr M, Johnson Y, Amofah B, Ye X, et al. Improving dual targeting selectivity in T-cell engagers via synapse-gated and affinity-tuned trispecific antibody design. MAbs. 2025;17(1):2570748. doi: 10.1080/19420862.2025.2570748.
14. Sebastiao MJ, Hoffman M, Escandell J, Tousi F, Zhang J, Figueroa B, DeMaria C, Gomes-Alves P. Identification of mispairing omic signatures in Chinese hamster ovary (CHO) cells producing a tri-specific antibody. Biomedicines. 2023;11(11):2890. doi: 10.3390/biomedicines11112890.
15. Gong D, Riley TP, Bzymek KP, Correia AR, Li D, Spahr C, Robinson JH, Case RB, Wang Z, Garces F. Rational selection of building blocks for the assembly of bispecific antibodies. MAbs. 2021;13(1):1870058. doi: 10.1080/19420862.2020.1870058.
16. Carter P. Bispecific human IgG by design. J Immunol Methods. 2001;248(1–2):7–15. doi: 10.1016/S0022-1759(00)00339-2.
17. Ridgway JB, Presta LG, Carter P. 'Knobs-into-holes' engineering of antibody CH3 domains for heavy chain heterodimerization. Protein Eng Des Sel. 1996;9(7):617–621. doi: 10.1093/protein/9.7.617.

18. Vaks L, Litvak-Greenfeld D, Dror S, Shefet-Carasso L, Matatov G, Nahary L, Shapira S, Hakim R, Alroy I, Benhar I. Design principles for bispecific IgGs, opportunities and pitfalls of artificial disulfide bonds. Antibodies (Basel). 2018;7(3):27. doi: 10.3390/antib7030027.
19. Bagert JD, Oganesyan V, Chiang C-I, Iannotti M, Lin J, Yang C, Payne S, McMahon W, Edwards S, Dippel A, et al. Robust production of monovalent bispecific IgG antibodies through novel electrostatic steering mutations at the C(H)1-C(lambda) interface. MAbs. 2023;15(1):2273449. doi: 10.1080/19420862.2023.2273449.
20. Merchant AM, Zhu Z, Yuan JQ, Goddard A, Adams CW, Presta LG, Carter P. An efficient route to human bispecific IgG. Nat Biotechnol. 1998;16(7):677–681. doi: 10.1038/nbt0798-677.
21. Brinkmann U, Kontermann RE. The making of bispecific antibodies. MAbs. 2017;9(2):182–212. doi: 10.1080/19420862.2016.1268307.
22. Mistry RK, Kelsall E, Sou SN, Barker H, Jenns M, Willis K, Zurlo F, Hatton D, Gibson SJ. A novel hydrogen peroxide evolved CHO host can improve the expression of difficult to express bispecific antibodies. Biotechnol Bioeng. 2021;118(6):2326–2337. doi: 10.1002/bit.27744.
23. Chakrabarti L, Chaerkady R, Wang J, Weng SHS, Wang C, Qian C, Cazares L, Hess S, Amaya P, Zhu J, et al. Mitochondrial membrane potential-enriched CHO host: a novel and powerful tool for improving biomanufacturing capability. MAbs. 2022;14(1):2020081. doi: 10.1080/19420862.2021.2020081.
24. Cartwright JF, Arnall CL, Patel YD, Barber NOW, Lovelady CS, Rosignoli G, Harris CL, Dunn S, Field RP, Dean G, et al. A platform for context-specific genetic engineering of recombinant protein production by CHO cells. J Biotechnol. 2020;312:11–22. doi: 10.1016/j.jbiotec.2020.02.012.
25. Gomez N, Barkhordarian H, Lull J, Huh J, GhattyVenkatakrishna P, Zhang X. Perfusion CHO cell culture applied to lower aggregation and increase volumetric productivity for a bispecific recombinant protein. J Biotechnol. 2019;304:70–77. doi: 10.1016/j.jbiotec.2019.08.001.
26. Peltret M, Vetsch P, Farvaque E, Mette R, Tsachaki M, Duarte L, Duret A, Vaxelaire E, Frank J, Moritz B, et al. Development of a 10 g/l process for a difficult-to-express multispecific antibody format using a holistic process development approach. J Biotechnol. 2024;389:30–42. doi: 10.1016/j.jbiotec.2024.04.017.
27. Lambiase G, Klottrup-Rees K, Lovelady C, Ali S, Shepherd S, Muroni M, Lindo V, James DC, Dickman MJ. An automated, low volume, and high-throughput analytical platform for aggregate quantitation from cell culture media. J Chromatogr A. 2023;1691:463809. doi: 10.1016/j.chroma.2023.463809.
28. Sou SN, Harris CL, Williams R, Kozub D, Zurlo F, Patel YD, Kallamvalli Illam Sankaran P, Daramola O, Brown A, James DC, et al. Cho synthetic promoters improve expression and product quality of biotherapeutic proteins. Biotechnol Prog. 2023;39(5):e3348. doi: 10.1002/btpr.3348.
29. Ong HK, Nguyen NTB, Bi J, Yang Y. Vector design for enhancing expression level and assembly of knob-into-hole based FabscFv-Fc bispecific antibodies in CHO cells. Antib Ther. 2022;5(4):288–300. doi: 10.1093/abt/tbac025.
30. Smith EJ, Olson K, Haber LJ, Varghese B, Duramad P, Tustian AD, Oyejide A, Kirshner JR, Canova L, Menon J, et al. A novel, native-format bispecific antibody triggering T-cell killing of B-cells is robustly active in mouse tumor models and cynomolgus monkeys. Sci Rep. 2015;5(1):17943. doi: 10.1038/srep17943.
31. Feige MJ, Groscurth S, Marcinowski M, Shimizu Y, Kessler H, Hendershot LM, Buchner J. An unfolded CH1 domain controls the assembly and secretion of IgG antibodies. Mol Cell. 2009;34(5):569–579. doi: 10.1016/j.molcel.2009.04.028.
32. Gong S, Wu C. Efficient production of bispecific antibodies-optimization of transfection strategy leads to high-level stable cell line generation of a fabs-in-tandem immunoglobin. Antib Ther. 2023;6(3):170–179.
33. Kelsall E, Harris C, Sen T, Hatton D, Dunn S, Gibson S. Interplay of heavy chain introns influences efficient transcript splicing and affects product quality of recombinant biotherapeutic antibodies from CHO cells. MAbs. 2023;15(1):2242548. doi: 10.1080/19420862.2023.2242548.
34. Liu S, Chen Q, Peng L, Li H, Zhao B, Wu M, Kang Y, Hu T, Guo X, Cao Y, et al. Tailoring plasmid design based on chain expression in cell line development for enhanced monoclonal and bispecific antibody production. Biotechnol J. 2025;20(8):e70104. doi: 10.1002/biot.70104.
35. Maltais JS, Lord-Dufour S, Morasse A, Stuible M, Loignon M, Durocher Y. Repressing expression of difficult-to-express recombinant proteins during the selection process increases productivity of CHO stable pools. Biotechnol Bioeng. 2023;120(10):2840–2852. doi: 10.1002/bit.28435.
36. Yang Y, Li Z, Li Q, Ma K, Lin Y, Feng H, Wang T. Increase recombinant antibody yields through optimizing vector design and production process in CHO cells. Appl Microbiol Biotechnol. 2022;106(13):4963–4975. doi: 10.1007/s00253-022-12051-5.
37. Patel YD, Brown AJ, Zhu J, Rosignoli G, Gibson SJ, Hatton D, James DC. Control of multigene expression stoichiometry in mammalian cells using synthetic promoters. ACS Synth Biol. 2021;10(5):1155–1165. doi: 10.1021/acssynbio.0c00643.
38. Mazor Y, Oganesyan V, Yang C, Hansen A, Wang J, Liu H, Sachsenmeier K, Carlson M, Gadre DV, Borrok MJ, et al. Improving target cell specificity using a novel monovalent bispecific IgG design. MAbs. 2015;7(2):377–389. doi: 10.1080/19420862.2015.1007816.
39. Eisenhut P, Mebrahtu A, Moradi Barzadd M, Thalén N, Klanert G, Weinguny M, Sandegren A, Su C, Hatton D, Borth N, et al. Systematic use of synthetic 5'-utr RNA structures to tune protein translation improves yield and

quality of complex proteins in mammalian cell factories. Nucleic Acids Res. 2020;48(20):e119. doi: 10.1093/nar/gkaa847.
40. Oliviero C, Hinz SC, Bogen JP, Kornmann H, Hock B, Kolmar H, Hagens G. Generation of a host cell line containing a MAR-rich landing pad for site-specific integration and expression of transgenes. Biotechnol Prog. 2022;38(4):e3254. doi: 10.1002/btpr.3254.
41. Yamaguchi K, Ogawa R, Tsukahara M, Kawakami K. Production of multi-subunit proteins in CHO cells by transposase-mediated integration of subunit-splitting vectors. Sci Rep. 2025;15(1):18512. doi: 10.1038/s41598-025-03301-3.
42. Atwell S, Ridgway JBB, Wells JA, Carter P. Stable heterodimers from remodeling the domain interface of a homodimer using a phage display library. J Mol Biol. 1997;270(1):26–35. doi: 10.1006/jmbi.1997.1116.
43. Wang B, Albanetti T, Miro-Quesada G, Flack L, Li L, Klover J, Burson K, Evans K, Ivory W, Bowen M, et al. High-throughput screening of antibody-expressing CHO clones using an automated shaken deep-well system. Biotechnol Prog. 2018;34(6):1460–1471. doi: 10.1002/btpr.2721.
44. Chen S, Zhou Y, Chen Y, Gu J. Fastp: an ultra-fast all-in-one FASTQ preprocessor. Bioinformatics. 2018;34(17):i884–i890. doi: 10.1093/bioinformatics/bty560.
45. Patro R, Duggal G, Love MI, Irizarry RA, Kingsford C. Salmon provides fast and bias-aware quantification of transcript expression. Nat Methods. 2017;14(4):417–419. doi: 10.1038/nmeth.4197.
46. Srivastava A, Malik L, Sarkar H, Zakeri M, Almodaresi F, Soneson C, Love MI, Kingsford C, Patro R. Alignment and mapping methodology influence transcript abundance estimation. Genome Biol. 2020;21(1):239. doi: 10.1186/s13059-020-02151-8.
47. Howe KL, Achuthan P, Allen J, Allen J, Alvarez-Jarreta J, Amode MR, Armean IM, Azov AG, Bennett R, Bhai J, et al. Ensembl 2021. Nucleic Acids Res. 2020;49(D1):D884–D891. doi: 10.1093/nar/gkaa942.
48. Soneson C, Love M, Robinson M. Differential analyses for RNA-seq: transcript-level estimates improve gene-level inferences. F1000Res. F1000Research, 2015;4:1521. doi: 10.12688/f1000research.7563.1.
49. Ewels PA, Peltzer A, Fillinger S, Patel H, Alneberg J, Wilm A, Garcia MU, Di Tommaso P, Nahnsen S. The nf-core framework for community-curated bioinformatics pipelines. Nat Biotechnol. 2020;38(3):276–278. doi: 10.1038/s41587-020-0439-x.
50. Di Tommaso P, Chatzou M, Floden EW, Barja PP, Palumbo E, Notredame C. Nextflow enables reproducible computational workflows. Nat Biotechnol. 2017;35(4):316–319. doi: 10.1038/nbt.3820.
51. Dobin A, Davis CA, Schlesinger F, Drenkow J, Zaleski C, Jha S, Batut P, Chaisson M, Gingeras TR. Star: ultrafast universal RNA-seq aligner. Bioinformatics. 2012;29(1):15–21. doi: 10.1093/bioinformatics/bts635.
52. Zhang Y, Parmigiani G, Johnson WE. ComBat-seq: Batch effect adjustment for RNA-seq count data. NAR Genomics Bioinf. 2020;2(3). doi: 10.1093/nargab/lqaa078.
53. Love MI, Huber W, Anders S. Moderated estimation of fold change and dispersion for RNA-seq data with DESeq2. Genome Biol. 2014;15(12):550. doi: 10.1186/s13059-014-0550-8.